Shock Waves (1999) 9: 381–390

Shock Waves

Multi-dimensional hydrodynamic code SOVA for interfacial flows: Application to the thermal layer effect

V.V. Shuvalov

Russian Academy of Sciences, Institute for Dynamics of Geospheres, 38 Leninsky Prosp. (bldg. 6), Moscow, 117979, Russia

Received 15 June 1998/ Accepted 6 January 1999

Abstract. Eulerian, three-dimensional, numerical code, which conserves mass, momentum and energy simultaneously both in the Lagrangian and remap steps, is developed. The use of special form of linear viscosity provides a weaker time step restriction as compared with the Courant condition. The code is designed to investigate the multi-material problems, including dusty flows. The performance of the code is illustrated by the modeling of shock wave interaction with a dusty thermal layer.

Key words: Numerical code, Shock wave, Dust particles, Thermal layer

1 Introduction

The SOVA code was developed to model multi-dimensional, multi-material, gasdynamic flows including those contaminated by dust particles. The Eulerian forms of the governing equations are solved in two steps: a Lagrangian step and a remap step. In the first step the Lagrangian forms of equations are solved, then the distorted cells are remapped back to initial mesh (or some new mesh changing in time). The two-step procedure is more suitable for multi-material problems. A solution scheme similar to that used in the CTH System (McGlaun et al. 1990) is exploited to integrate the problem through time. But several principal advances are made.

The finite volume approximations of the conservation equations have been designed to conserve mass, momentum and energy both across the Lagrangian and remap steps. It is not a simple task if a non-divergence form of the energy equation is used. The main problem is to conserve the mass, momentum and kinetic energy across the remap, because these three quantities are usually calculated using two equations. From the physical point of view it means that a coupling of two or three volumes in the process of remapping is similar to nonelastic impact (the velocities becomes equal). This leads to a deficiency in the kinetic energy. In some codes this energy discrepancy is transformed into heat (McGlaun et al. 1990). However this procedure is not quite correct, though it provides a conservation of the total energy. Two opposite processes take place in fact at each time step: a coupling and separation of finite volumes. The kinetic energy (and momentum) distribution between the parts of separating volume should be determined from conservation conditions for coupling and separation simultaneously. An attempt to provide such a conservation is made in the SOVA code.

One more substantial advancement is the consideration of dust particles transfer in the frame of multi-material code. This makes the SOVA code related to a wider range of gasdynamical and geophysical applications.

The solution scheme and all the details of the code are described in section two. The performance of the code is illustrated by modeling of shock wave interaction with dusty thermal layer. The results of this modeling are discussed in section three, followed by conclusions in section four.

2 Description of the code

2.1 Computational mesh and variable positions

Three-dimensional rectangular and two-dimensional cylindrical and rectangular geometries are used to generate the computational mesh. Each cell (i, j, k) is restricted by spatial coordinates: $x_i \le x \le x_{i+1}$, $y_j \le y \le y_{j+1}$, $z_k \le z \le z_{k+1}$ (for the 3D case). All quantities are cell centered except the velocities, which are centered on appropriate cell faces (see Fig. 1). A staggered mesh is constructed for the momentum conservation equation. The staggered cell boundaries pass through midpoints of the adjacent cells, so the mass of staggered cell equals one half the mass of two adjacent cells.

The process of multi-dimensional equation integration is simplified by using operator splitting techniques which replaces the multi-dimensional equations with a set of one-dimensional equations. This techniques is used both in the Lagrangian and remap steps. The operator splitting technique is also used to separate gasdynamic and gas-dust interaction steps.

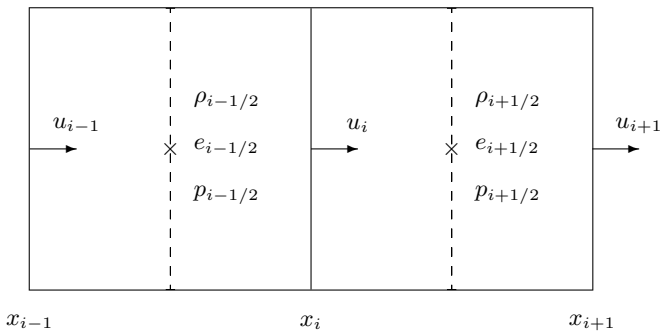

Fig. 1. Original (*solid lines*) and staggered (*dashed lines*) mesh and variable positions

2.2 Lagrangian step

Non-divergence form of energy equation is used for the numerical approximation. Therefore special efforts should be undertaken to conserve the total energy (McGlaun et al. 1990). The use of alternative conservative form of the energy equation provides the energy conservation automatically but leads to difficulties in the case of nearly inertial flows, where a small value of thermal energy is determined as a difference between two large values of the total and kinetic energies. The one-dimensional rectangular geometry forms of the finite volume equations are

$$\tilde{\rho}_{i+1/2}(\tilde{x}_{i+1}-\tilde{x}_i)=\rho^n_{i+1/2}(x^n_{i+1}-x^n_i), \tag{1}$$

$$\tilde{x}_i = x^n_i + 0.5(u^n_i+\tilde{u}_i)\tau, \tag{2}$$

$$\frac{\tilde{u}_i-u^n_i}{\tau} + \frac{p_{i+1/2}-p_{i-1/2}}{0.5(\rho^n_{i-1/2}(x^n_i-x^n_{i-1})+\rho^n_{i+1/2}(x^n_{i+1}-x^n_i))}=0, \tag{3}$$

$$\frac{\tilde{e}_{i+1/2}-e^n_{i+1/2}}{\tau} + p_{i+1/2}\frac{u^n_{i+1}+\tilde{u}_{i+1}-u^n_i-\tilde{u}_i}{2\rho^n_{i+1/2}(x^n_{i+1}-x^n_i)}=0, \tag{4}$$

where ρ, e, p, u are the cell average density, thermal energy, pressure and velocity respectively, τ is the time step, index n corresponds to the values at the time level n, and the tilde marks the values at the end of the Lagrangian step. Such a form of approximation provides energy conservation if the same value of pressure is used in both Eqs. (3) and (4) (Popov and Samarsky, 1980).

The pressure $p_{i+1/2}$ is obtained by extrapolation from time level n to $n+1/2$ assuming that the entropy s remains constant (Barhrah et al. 1981)

$$p_{i+1/2}=p^n_{i+1/2}+\left(\frac{\partial p}{\partial \rho}\right)_S \frac{\partial \rho}{\partial t}\frac{\tau}{2}. \tag{5}$$

This expression can be rewritten as

$$p_{i+1/2}=p^n_{i+1/2}-\rho^n_{i+1/2}\left(c^n_{i+1/2}\right)^2\frac{\tilde{u}_{i+1}-\tilde{u}_i}{x_{i+1}-x_i}\frac{\tau}{2}, \tag{6}$$

where c is the sound speed. The second term in this formula may be treated as an implicit linear viscosity form. Involving of the velocities from $n+1$ time level increases the stability of the scheme. As a result the time step τ is restricted not by Courant conditions but by a weaker condition

$$\tau \le \min\left(\min_i \frac{x_{i+1}-x_i}{|u_i|}, \min_i \frac{x_i-x_{i-1}}{|u_i|}\right). \tag{7}$$

Equation (3) with the pressure (6) is solved using a sweep method (Oran and Boris, 1987). Quadratic artificial viscosity is used to model shocks.

Equations (1-4) define the total thermal energy and density in the cell. If the cell contains more than one material, thermodynamic parameters of each component are determined from the following equations:

$$p_l(\tilde{e}_l,\tilde{\rho}_l)=p_m(\tilde{e}_m,\tilde{\rho}_m) \qquad \forall l,m, \tag{8}$$

$$\sum_m \alpha_m\tilde{\rho}_m=\tilde{\rho}, \tag{9}$$

$$\tilde{e}_m = e^n_m + p\left(\frac{1}{\tilde{\rho}_m}-\frac{1}{\rho_m}\right), \tag{10}$$

where l and m are material numbers, α is material volume concentration and p is defined by (6).

2.3 Remap step

The velocities, densities and energies updated at the Lagrangian step must be remapped to the initial (or some other) mesh. The second order Van Leer scheme (Van Leer, 1977) replacing a uniform distribution in the donor cell with a linear distribution is used to remap density and internal energy. The mass, momentum and kinetic energy cannot be conserved simultaneously if the same procedure is applied to calculate the velocity. For this reason a special algorithm is used for the velocity remapping. The momentum and kinetic energy exchange between two adjacent cells is described by conservation laws:

$$m^n_i\tilde{\tilde{u}}_i + m^n_{i+1}\tilde{u}_{i+1} = (m^n_i-\triangle m)u^{n+1}_i + (m^n_{i+1}+\triangle m)\tilde{\tilde{u}}_{i+1}, \tag{11}$$

$$m^n_i(\tilde{\tilde{u}}_i)^2 + m^n_{i+1}(\tilde{u}_{i+1})^2 = (m^n_i-\triangle m)(u^{n+1}_i)^2 + (m^n_{i+1}+\triangle m)(\tilde{\tilde{u}}_{i+1})^2, \tag{12}$$

where m is a staggered cell mass, $\triangle m$ is a mass flux across a cell face, $\tilde{\tilde{u}}_i$ is the velocity obtained after momentum-energy exchange between $i-1$ and i cells. The resulting equations are:

$$u^{n+1}_i = \frac{m^n_i\tilde{\tilde{u}}_i + m^n_{i+1}\tilde{u}_{i+1}}{m^n_i+m^n_{i+1}} + \frac{\tilde{\tilde{u}}_i-\tilde{u}_{i+1}}{m^n_i+m^n_{i+1}} \times\sqrt{\frac{(m^n_{i+1}+\triangle m)m^n_i m^n_{i+1}}{m^n_i-\triangle m}}, \tag{13}$$

$$\tilde{\tilde{u}}_{i+1} = \frac{m^n_i\tilde{\tilde{u}}_i + m^n_{i+1}\tilde{u}_{i+1}}{m^n_i+m^n_{i+1}} + \frac{\tilde{u}_{i+1}-\tilde{\tilde{u}}_i}{m^n_i+m^n_{i+1}} \times\sqrt{\frac{(m^n_i-\triangle m)m^n_i m^n_{i+1}}{m^n_{i+1}+\triangle m}}. \tag{14}$$

For $\triangle m \ll m_i^n$ and $\triangle m \ll m_{i+1}^n$ Eq. (13) leads to the momentum flux $\triangle m(\tilde{\tilde{u}}_i + \tilde{u}_{i+1})/2$, which corresponds to the second order of accuracy. This procedure is not symmetric, different results are obtained in the cases where index i increases or decreases. The asymmetry is minimized by permuting the direction of calculations.

The algorithm described above provides the conservation of all physical quantities, it is totally conservative according to terminology of Popov and Samarsky (1980).

Some interface reconstruction techniques are necessary to remap density and internal energy in the case of multimaterial cells. The SLIC scheme (Noh and Woodward, 1976) is used in SOVA for three-dimensional mesh. The high resolution interface tracker developed in CTH (McGlaun et al. 1990) is exploited in the case of two-dimensional geometry.

2.4 Dusty flow modeling

Two techniques may be used to solve equations of dust particles motion. The first one is based on the same finite volume approximation as used for integration of the equations for gas component (i.e. Valentine and Wohletz, 1989). This assumption treats the particles of each size as a fluid having its own velocity (the same for all closely spaced particles), density, thermal energy and zero pressure. This approach is rather simple, but has some limitations such as strong discreteness of particles' size distribution and uncontrollable numerical diffusion. Another disadvantage is the impossibility of having different velocities for grains having the same size and close coordinates. This may lead to unreliable particle accumulation in the case of flows striking together (Rodionov, 1996).

The second techniques (Boothroyd, 1971), used in SOVA, are based on solving equations of motion for some number ($10^3 \div 10^5$) of representative particles (markers). Each of these markers represents the motion of a large number ($10^5 \div 10^{10}$) of real dust grains having close trajectories. The Monte Carlo method is used to calculate the diffusion spreading of the dust. The replacement $\delta\mathbf{r}$ of the particle at each time step is defined as $\delta\mathbf{r} = \mathbf{u}\tau + \mathbf{j}\sqrt{6D\tau}$, where D is the coefficient of diffusion and $\mathbf{j}$ is a unit vector in accidental direction.

The motion of a representative particle with the mass m_i, diameter d_i and velocity $\mathbf{u}_i$ in a gravitational field is governed by equation

$$m_i \frac{d\mathbf{u}_i}{dt} = m_i\mathbf{g} + 3\pi d_i\mu(\mathbf{u}_g - \mathbf{u}_i)$$

$$+\frac{1}{4}C_d\pi d_i^2\rho_g|\mathbf{u}_g - \mathbf{u}_i|(\mathbf{u}_g - \mathbf{u}_i), \qquad (15)$$

where $\mathbf{g}$ is gravity, $\mathbf{u}_g$ and ρ_g are gas velocity and density, C_d is a drag coefficient and μ is the viscosity coefficient. The first term on the right hand describes gravity action, the second and third ones represent low-speed flow regime Stokes drag and high-speed flow regime form drag. This vector equation is broken into scalar component equations. For brevity two-dimensional equations are considered below. An extension to the 3D case is trivial. If z is a vertical coordinate and r is a horizontal one then

$$\frac{du_{iz}}{dt} = -g + a_{1i}(u_{gz} - u_{iz})$$

$$+a_{2i}|\mathbf{u}_g - \mathbf{u}_i|(u_{gz} - u_{iz}), \qquad (16)$$

$$\frac{du_{ir}}{dt} = a_{1i}(u_{gr} - u_{ir})$$

$$+a_{2i}|\mathbf{u}_g - \mathbf{u}_i|(u_{gr} - u_{ir}), \qquad (17)$$

where

$$a_{1i} = \frac{3\pi d_i\mu}{m_i}, \qquad a_{2i} = \frac{C_d\pi d_i^2\rho_g}{4m_i}. \qquad (18)$$

An implicit procedure must be used to obtain the correct limits at $\tau \to \infty$. Eq. (17) is approximated as

$$\frac{u_{ir}^{n+1} - u_{ir}^n}{\tau} = a_{3i}(u_{gr}^{n+1} - u_{ir}^{n+1}),$$

$$a_{3i} = a_{1i} + a_{2i}|\mathbf{u}_g^n - \mathbf{u}_i^n|, \qquad (19)$$

which leads to the following expression for the new particle velocity:

$$u_{ir}^{n+1} = a_{4i} + a_{5i}u_{gr}^{n+1}, \qquad (20)$$

where

$$a_{4i} = \frac{u^n}{1 + \tau a_{3i}}, \qquad a_{5i} = \frac{\tau a_{3i}}{1 + \tau a_{3i}}. \qquad (21)$$

The value of updated gas velocity u_{gr}^{n+1} is defined from the equation of momentum conservation:

$$m_g u_{gr}^n + \sum m_i u_{ir}^n =$$

$$m_g u_{gr}^{n+1} + \sum m_i(a_{4i} + a_{5i}u_{gr}^{n+1}), \qquad (22)$$

with summation over all the particles situated within the grid cell with a mass m_g.

A more complicated procedure is applied for vertical velocity calculations to provide a passage to the limit to the sedimentation velocity at high time step. Different approximations are used for the cases of $u_{gz}^n > u_{iz}^n$ and $u_{gz}^n < u_{iz}^n$. In the first case let u_{0i} be the solution of the equation

$$-g + a_{1i}x + \tilde{a}_{2i}x^2 = 0, \qquad (23)$$

where

$$\tilde{a}_{2i} = min(a_{2i}\frac{|\mathbf{u}_g^n - \mathbf{u}_i^n|}{u_{gz}^n - u_{iz}^n}, \beta a_{2i}). \qquad (24)$$

Here β is a rather big constant, for example, 100. For the case of $u_{gr}^n - u_{ir}^n = 0$ the value of u_{0i} coincides with the velocity of stationary sedimentation.

A combination of (16) and (23) gives an equation

$$\frac{du_{iz}}{dt} = (u_{gz} - u_{iz} + u_0)$$

$$[a_{1i} + \tilde{a}_{2i}(u_{gz} - u_{iz} - u_{0i})]. \qquad (25)$$

It is approximated as

$$\frac{u_{iz}^{n+1}-u_{iz}^{n}}{\tau}=a_{3i}(u_{gz}^{n+1}-u_{iz}^{n+1}+u_{0i}),$$

$$a_{3i}=a_{1i}+\tilde{a}_{2i}(u_{gz}^{n}-u_{iz}^{n}-u_{0i}), \tag{26}$$

which leads to the updated particle velocity in the form:

$$u_{iz}^{n+1}=a_{4i}+a_{5i}u_{gz}^{n+1}, \tag{27}$$

where

$$a_{4i}=\frac{u_{iz}^{n}+\tau a_{3i}u_{0i}}{1+\tau a_{3i}},\qquad a_{5i}=\frac{\tau a_{3i}}{1+\tau a_{3i}}. \tag{28}$$

In the case of $u_{gz}^{n}<u_{iz}^{n}$ Eq. (16) is approximated in the same way as the equation for the horizontal velocity:

$$\frac{u_{iz}^{n+1}-u_{iz}^{n}}{\tau}=-g+[a_{1i}-a_{2i}|\mathbf{u}_g^n-\mathbf{u}_i^n|](u_{gz}^{n+1}-u_{iz}^{n+1})$$
$$=-g+a_{3i}(u_{gz}^{n+1}-u_{iz}^{n+1}), \tag{29}$$

which gives

$$u_{iz}^{n+1}=a_{4i}+a_{5i}u_{gz}^{n+1} \tag{30}$$

with

$$a_{4i}=\frac{u_{iz}^{n}-g\tau}{1+\tau a_{3i}},\qquad a_{5i}=\frac{\tau a_{3i}}{1+\tau a_{3i}}. \tag{31}$$

The value of updated gas velocity u_{gz}^{n+1} is determined from the equation of momentum conservation

$$m_g u_{gz}^{n}+\sum m_i(u_{iz}^{n}-g\tau)$$

$$=m_g u_{gz}^{n+1}+\sum m_i(a_{4i}+a_{5i}u_{gz}^{n+1}). \tag{32}$$

Dust particle replacement is defined from

$$z_i^{n+1}=z_i^{n}+0.5(u_{iz}^{n}+u_{iz}^{n+1})\tau, \tag{33}$$

$$r_i^{n+1}=r_i^{n}+0.5(u_{ir}^{n}+u_{ir}^{n+1})\tau, \tag{34}$$

where (z_i^n, r_i^n) and (z_i^{n+1}, r_i^{n+1}) are particle old and new coordinates.

A gas-particle interaction is a nonelastic process which causes a transformation of a portion of kinetic energy into thermal energy. The value of gas heating $\triangle e$ is defined as

$$\triangle e=\frac{1}{2}m_g|\mathbf{u}_g^n|^2+\frac{1}{2}\sum m_i|\mathbf{u}_i^n|^2-\frac{1}{2}m_g|\mathbf{u}_g^{n+1}|^2$$
$$-\frac{1}{2}\sum m_i|\mathbf{u}_i^{n+1}|^2-\sum m_i g(z_i^{n+1}-z_i^{n}). \tag{35}$$

An interphase heat transfer due to radiation and forced convection is defined by the expression

$$Q_i=-\frac{6\theta_i\sigma}{d_i}[e_iT_i^4-a_gT_g^4]$$
$$-\frac{6\theta_i K_g}{d_i^2}[2.0+0.6Re_i^{1/2}Pr_g^{1/3}](T_i-T_g), \tag{36}$$

where θ_i is the ratio of particles' volume to the cell volume, Pr and Re are Prandtl and Reynolds numbers, σ is the Stefan-Boltzmann constant, a_g and e_i are the absorptivity of the gas and the emissivity of the particles, T is the temperature, and K_g is the thermal conductivity (see, for example, Valentine and Wohletz, 1989). If necessary an implicit procedure similar to that described above for the velocity updating is used to solve (36).

When a particle moves through a cell containing different materials the drag is determined by the density of the material surrounding the particle at the moment. But crossing a cell the particle successively passes all the materials, and in the mean the time of moving through every component is proportional to the component volume concentration. Thus the time average drag may be calculated using a space average cell density.

Similarly the heat exchange between every particle and multi-material cell is calculated under the assumption that at each time step τ the particle contacts with each material through the time $\alpha_i\tau$, where α_i is the volume concentration of the i-th material.

To calculate the gas-dust interaction one should first find all the particles contained within every cell. This procedure would be very time consuming if being implemented directly, by sorting all the particles for each cell. To diminish the time expense at the beginning of each time step the particles are arranged in the order they are used in the process of calculation. A very fast sorting algorithm (heapsort) is applied to do this.

The algorithm described above provides fast operation, high accuracy and correct approximation for limiting cases.

3 Numerical simulations of the thermal layer effect

The thermal layer effect was discovered in the middle 50's in the course of nuclear tests (Glasstone and Dolan, 1977; Sadovsky and Adushkin, 1988). The effect shows itself as a growing precursor formation ahead of the blast wave, which causes a global change of the flow behind the shock. The precursor arises in the process of shock wave interaction with a thin layer of low density (thermal layer). The general discussion of this phenomenon had been provided by Shreffler and Christian (1954), Griffith (1956), Hess (1957), Taganov (in Gubkin, 1970). A criterion of precursor arising was derived. Later theoretical and experimental investigations were continued by Tsikulin and Popov (1977), Mirels (1988), Nemtchinov et al. (1987, 1989), Kuhl and Reichenbach(1988) and others. In particular it was shown that the precursor rises linearly with time and self-similarly (Nemtchinov et al., 1987). As this takes place the rate of precursor growth does not depend on the thermal layer (TL) thickness.

3.1 Results of numerical simulations

The first set of present numerical simulations was directed to reproduce the results of Nemtchinov et al. (1987) in

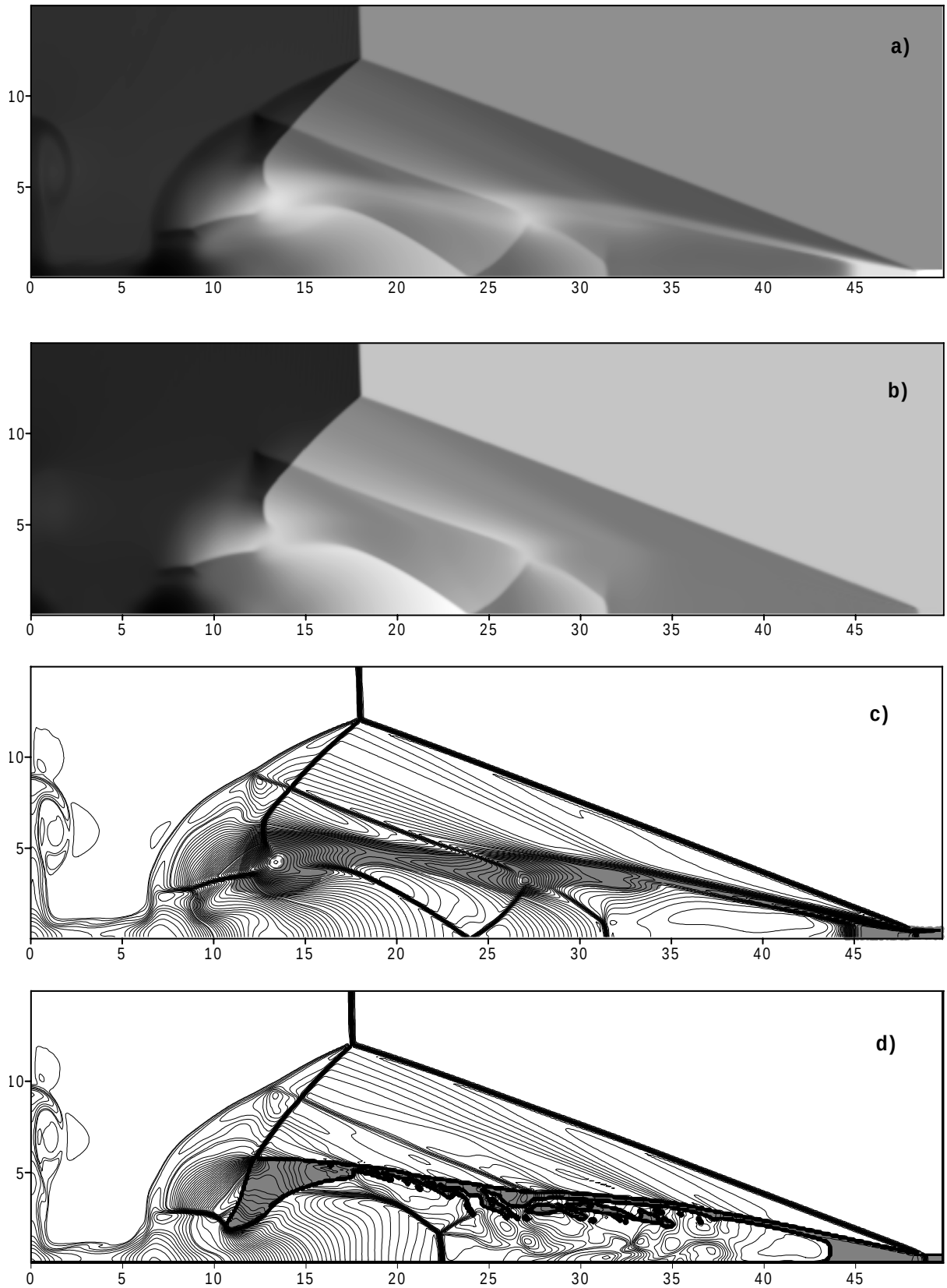

Fig. 2a–d. Density **a**, pressure **b** and TL material **c,d** distributions in the planar piston problem with the nondusty heated layer. **a,b,c** correspond to one-material problem, the distribution **d** was obtained by the two-material problem

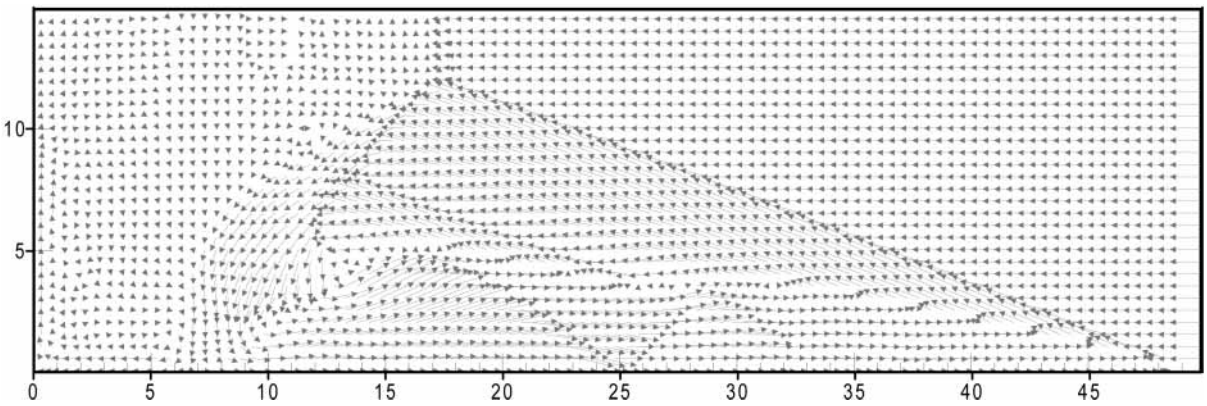

Fig. 3. The velocity field corresponding to density and pressure distribution presented in Fig. 2

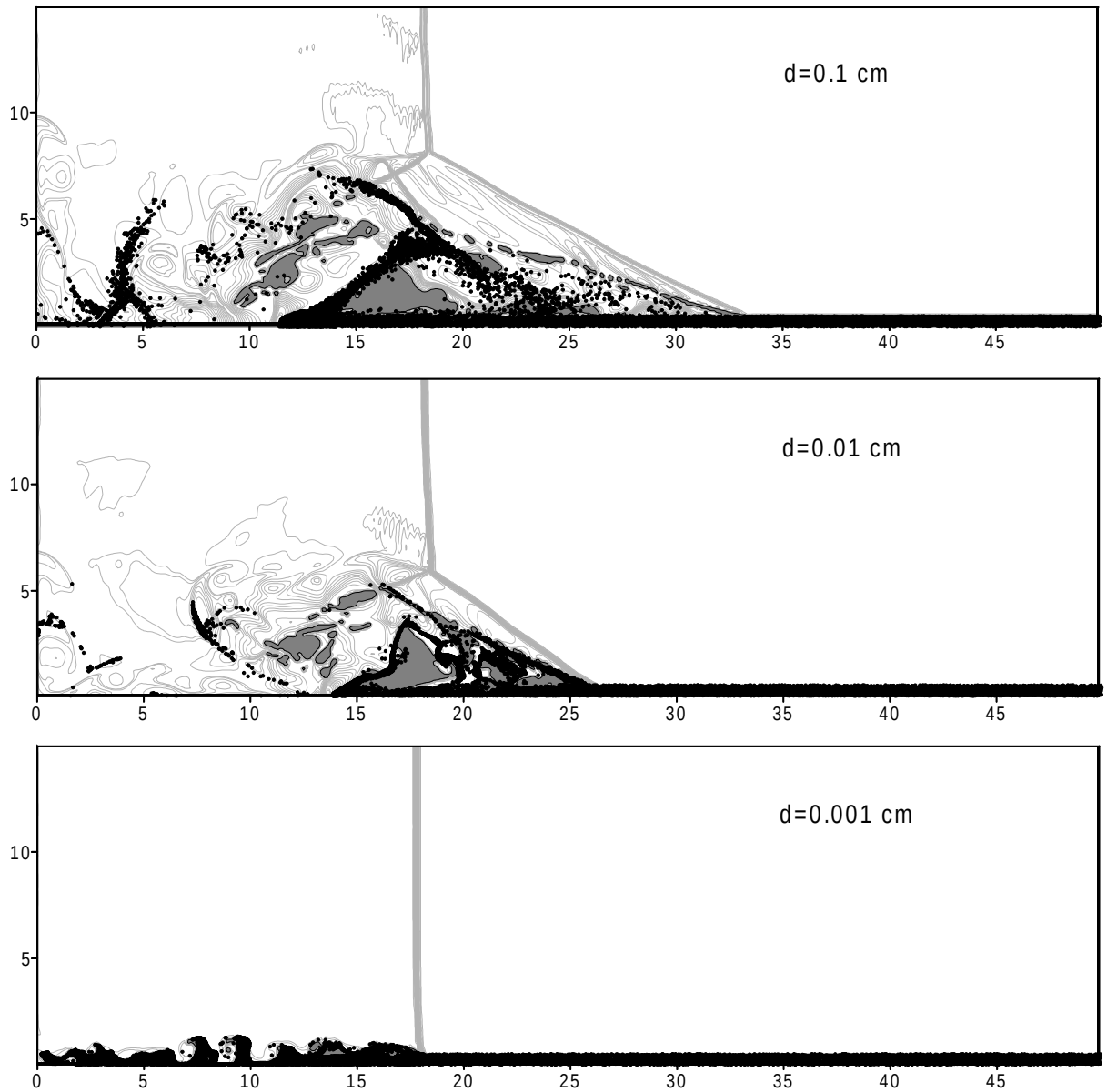

Fig. 4. Density isolines, dust particles (*dots*) and TL material (*gray shading*) distributions obtained in the runs with different values of particles' diameter d

more detail and to follow the trajectory of TL material. A planar shock wave created by a piston moving through the air of normal density with constant velocity V was considered. The thickness of the heated layer equals 0.5 m, and the characteristic scale of the problem is 100 m, which is typical for nuclear explosions and small asteroid impacts (Adushkin and Nemtchinov, 1994). Ideal gas equation of state was applied to calculate the air pressure. Computational mesh consisted of 200×500 cells with 5 cells across the thermal layer.

The results for $V = 1$ km/s (Mach number $M = 3$) and TL rarefaction $\omega = 0.1$ are shown in Figs. 2–3. Figure 2a,b demonstrate density and pressure distributions at the moment $t = 0.066$ s for the one-material problem. More intense shading corresponds to larger values. Figure 3 shows the velocity field (in the frame referred to the piston) for the same run. Due to lower density (and higher sound speed) the wave propagates more rapidly along the TL. This leads to formation of an oblique shock wave expanding from the surface. As a result an upward flow is formed within the precursor, which removes shock compressed TL material from the ground surface. A portion of the air from behind the main blast wave flows into the rarefied region.

More extensive computational mesh and better graphics allowed to obtain more complicated flow pattern than that presented in (Nemtchinov et al. 1987). Aside from the main vortex disposed left and below the three-shock point there is another one in the middle of the precursor (at $x = 27$ in Fig. 2). The interaction of the flow from behind the main blast wave with this second vortex results in formation of several more shock discontinuities near the surface. Most likely this configuration is rather stable in time. At least the increase of precursor size by 5-10 times is not accompanied with creation of new discontinuities.

Figure 2c demonstrates the distribution of marker particles initially situated within TL. This distribution was also obtained in the one-material problem. Figure 2d shows the results of the two-material simulation, where the ambient air and TL contained air were considered as two different materials, and the boundary between these was resolved. In general the results of the two problems agree with each other. Distributions of the TL material in both cases demonstrate the existence of the second vortex, where some portion of TL substance is torn apart. Some difference appears in the region between the middle vortex and the leading edge of the precursor. The flow pattern obtained in the two-material run allows to suppose turbulent mixing within the front part of the precursor (at $25 < x < 40$ in Fig. 2), where chaotic density perturbations are observed. Nevertheless the flow remains self-similar on the whole. The rate of precursor growth remains constant in time and the same as that obtained in the one-material problem.

The second set of simulations is directed to study the influence of aerosol particles on the appearance of TL effect, if such particles are involved into the heated layer in the process of its formation.

Dust entrainment due to TL effect induced vorticity was considered in (Kuhl et al. 1993; Rybakov et al. 1997). The purpose of the current investigation is to study the influence of dust on the precursor itself.

Actually temperature and dust density are not constant across the surface layer. For simplicity some limiting model cases are usually investigated (dust-free thermal layer with constant temperature, loose dust layer covered by clean uniform TL, etc). In this paper the interaction of the shock wave with thermal layer with uniformly distributed dust is considered.

The statement of the problem is the same as described above, but the particles of diameter d were disposed uniformly through TL. The summarized dust and air density equaled the density of the ambient air.

It is clear in advance that the particle size is critical for precursor evolution, because dust-gas interaction depends strongly on this size. Very small grains move with the same velocity as the gas, and dust-gas mixture in a sense behaves as a gas of summarized density. Therefore one may expect a steady flow without any precursor. If in contrast the particle size is great, the time of gas-dust velocity equalizing is also great. In this case the influence of dust is almost negligible.

But it is not clear in advance what kind of flow occurs for intermediate particles' sizes. It is also unclear whether the flow will be self-similar with a constant rate of precursor growth or the particles action will depend on the current precursor length. To answer these questions three runs with grain diameters $d = 10^{-3}, 10^{-2}$ and 10^{-1} cm were performed.

Figure 4 demonstrates density, dust and TL material distributions for all runs at the same moment of time $t = 0.066$ s. In the case of $d = 10^{-1}$ cm a well developed precursor is formed. But its length is about two times less than that in the case of noncontaminated TL. Dust particles move through the rarefied precursor almost not experiencing any drag. Some portion of heated gas is carried away by the particles, and remaining gas is removed from the ground by the flow created due to diagonal wave expansion. Dust grains are decelerated and torn apart (in the piston related frame) only under collision with the dense shock gas flowing from behind the main blast wave. It is this delay in particles deceleration which is responsible for the precursor formation.

A more complicated flow occurs in the case of smaller grains with $d = 10^{-2}$ cm. Some particles are entrained from the surface by the TL gas just behind the shock front in the heated layer. Other grains penetrate into the precursor and decelerate interacting with the air compressed by the main shock. Finally in both cases all the dust is blown off the ground and rises to the height which is comparable with the precursor vertical size.

At last, in the case of very small grains with $d = 10^{-3}$ cm a precursor does not appear at all. There is only a small disturbance of the size comparable with the TL thickness, and this disturbance does not grow in time. The dusty gas behaves as an ordinary gas of the same density as the ambient air. The values of sound speed are also close,

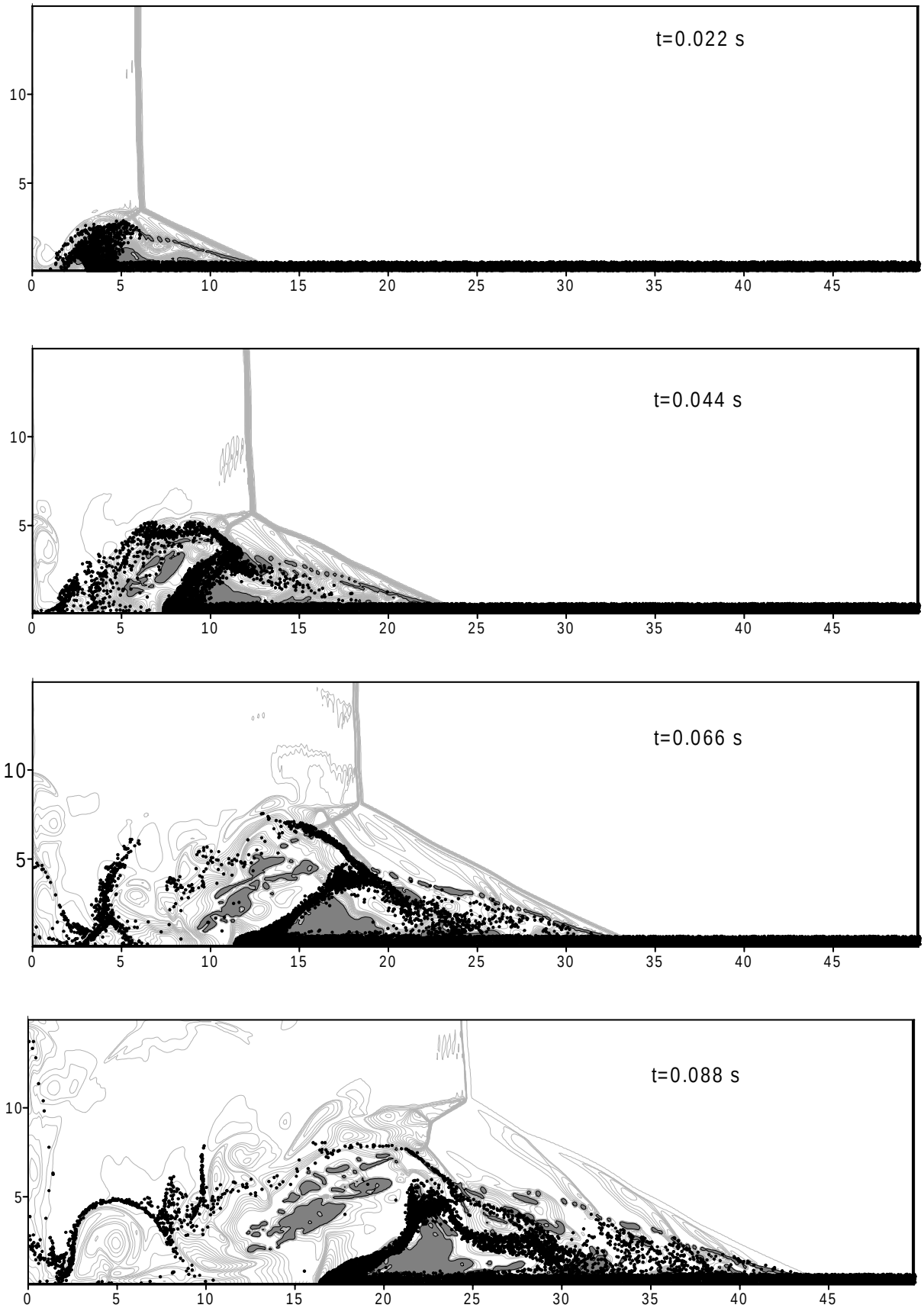

Fig. 5. The precursor evolution in the case of dust particles' diameter $d = 0.1$ cm. Density isolines, dust particles' distribution (*dots*) and TL material distribution (*gray shading*) are presented

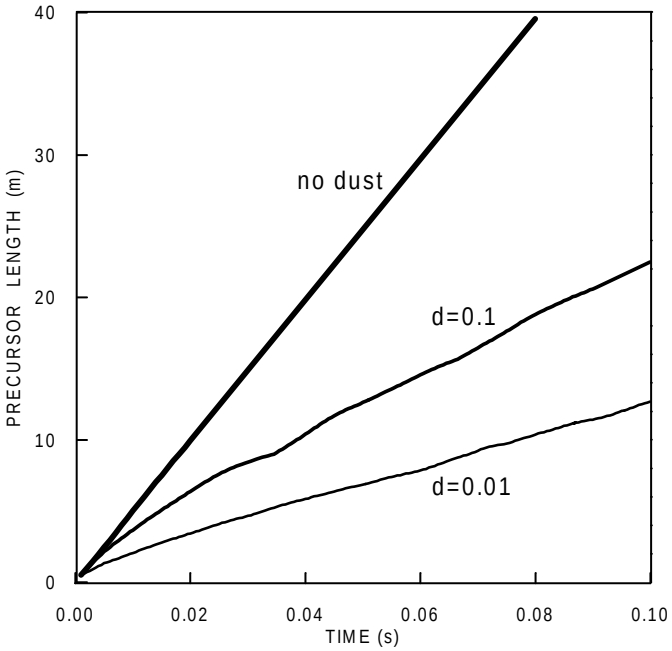

Fig. 6. Precursor length versus time for nondusty TL and dust particles measuring of 0.01 cm and 0.1 cm

but the values of $\gamma - 1$ (where γ is the specific heat ratio) differ noticeably from each other. This results in the different densities and velocities behind the shock. The dust layer behind the shock remains rather thin but it is considerably disturbed due to Kelvin-Helmholtz instability development at the boundary between dusty and pure air.

The temporal evolution of the precursor for the first run ($d = 10^{-1}$ cm) is shown in Fig. 5. After the first 0.022 s a typical precursor arises which does not contain dust particles except a thin layer near the ground. As the precursor length (and the time of particle-gas interaction consequently) increases some grains escape the surface layer before being decelerated by the dense air compressed in the main shock. The dust distribution and discontinuity structure considerably changes over time.

The time dependence of the precursor length is shown in Fig. 6. As demonstrated in (Nemtchinov et al. 1987) in the absence of dust the precursor increases linearly with time. For dusty TL this increase is also almost linear, although dust and TL material distributions slightly change in the process of precursor growth. The rate of precursor growth depends strongly on the particle size approaching the no-dust limit at high grain diameters.

3.2 Discussion

In the problem under consideration the low-speed viscous Stokes drag and gravity action may be neglected, because they are small in comparison with the high-speed flow regime drag. So Eq. (15) for particle deceleration may be replaced by

$$\frac{du_i}{dt} = -a_{2i}u_i^2, \qquad a_{2i} \simeq \frac{d_i\rho_g}{\rho_d}, \tag{37}$$

where ρ_d is the density of particle material, and u_i is the relative particle velocity. This gives the velocity relaxation law in the form

$$u_i = \frac{u_0}{1 + u_0 a_{2i} t}. \tag{38}$$

The time τ_* of velocity decrease by an order of magnitude is defined by relation

$$\tau_* \simeq 10\frac{d_i}{u_0}\frac{\rho_d}{\rho_g}. \tag{39}$$

For $u_0 = 1$ km/s, $\rho_g = 2 \cdot 10^{-4}$ g/cm^3 and dust substance density $\rho_d = 2.5$ g/cm^3 one can obtain $\tau_* = 10^{-1}, 10^{-2}$ and 10^{-3} s for $d = 10^{-1}, 10^{-2}$ and 10^{-3} cm respectively. This value should be compared with the time of particle passing through the region where TL substance is torn from the surface (a region from 44 m to 48 m at Fig. 2). This time equals $4 \cdot 10^{-3}$ s. The results of numerical simulations agree well with this estimate. It also follows from numerical simulations, that the size of the region where the TL gas rises from the ground surface does not change with time and depends on the TL air density and TL thickness only. From this results the conclusion that the dust influence on the precursor appearance depends on the TL thickness. This is a substantial difference from the TL effect appearance without dust, where the thickness of the heated layer does not influence the flow (Nemtchinov et al. 1987).

In the paper of Kuhl et al. (1993) an idea was suggested that the turbulence development may violate the self-similarity of the flow and even stop the precursor growth. The results of the present investigation argue an another (opposite) point of view presented in Nemtchinov et al. (1987). It follows from the numerical simulations described above that perturbations in the interior of the precursor, caused by instabilities development and dust action, do not influence the precursor growth. The rate of growth does not change in time if the shock velocity and TL parameters remain constant. To prove the flow's self-similarity one should investigate the solution as $\xi \to \infty$, where $\xi = MVt/H$ and H is the thermal layer thickness. Experiments of shock wave propagation along a hot (800 K) wall (Kuhl and Reichenbach, 1988) suggest that the wall jet breaks up at $\xi \simeq 300$ due to turbulent mixing. It follows from the present numerical simulations that the flow remains self-similar at least for $\xi \leq 200$. The results may depend on the spatial resolution of numerical modeling and experimental procedure. Thus the problem remains to be solved, and both additional theoretical investigations and experimental study are required for the progress to be made. It should be noted that this problem is not very important for point-like explosions because of the finite length of the TL (due to finite thermal energy of the source).

4 Conclusions

This work introduces a new multi-material, multi-dimensional hydrodynamic code SOVA, which allows to investigate a wide range of gasdynamical and geophysical problems. The mass, momentum and kinetic energy are conserved both across the Lagrangian and remap steps, although non-divergence form of the energy equation is used. Different forms of equation of state (analytical and tabularized) may be used. The code allows to study the flows contaminated by aerosol particles, which is important for many geophysical applications. Radiation effects are taken into account (in assumption of thermal conductivity) if necessary. Preliminary version of this code has already been used for modeling the Shoemaker-Levy 9 Comet collision with Jupiter (Nemtchinov et al. 1997; Shuvalov et al. 1997) and meteoroid impacts against the Moon (Nemtchinov et al. 1997).

In the present paper the performance of the SOVA code is illustrated by modeling a shock wave interaction with a dusty heated layer. It is shown that the appearance of the thermal layer effect (precursor parameters and even its creation) depends strongly on the dust particles' size. Nevertheless the flow remains self-similar over a considered period of time.

Acknowledgements. The author would like to thank Dr. Nataly Artem'eva and Irina Trubetskaya for their assistance with programming and preparing this paper; also to thank Dr. Vladimir V. Svettsov, Prof. Ivan V. Nemtchinov and Dr. Allen L. Kuhl for their valuable remarks.

References

Adushkin VV, Nemtchinov IV (1994) Consequences of impacts of cosmic bodies on surface of the Earth. In: Gehrels T (ed) Hazards due to Comets and Asteroids. Univ of Arizona Press, Tucson, Arizona, 721–778

Barhrah SM, Glagoleva YuP, Samugin MS, Frolov BD, Janenko NN, Janilkin YuV (1981) Calculations of gasdynamic flows on the base of concentration method. Docl Acad Nauk SSSR 257: 566–569 (in Russian)

Boothroyd RG (1971) Flowing gas-solids suspensions. Chapman and Hall Ltd., London

Glasstone S, Dolan PJ (1977) The effects of nuclear weapons. Washington, D.C.:GPO. p.653

Griffith WC (1956) Interaction of shock wave with a thermal boundary layer. J Aeronaut Sci vol.23 1: 16–23

Gubkin KE (1970) The propagation of blast waves. In: Mechanics in the USSR over 50 Years. Nauka, Moscow (in Russian)

Hess RV (1957) Interaction of moving shocks and hot layer. NACA TN 4002

Kuhl AL, Reichenbach H (1988) Techniques for creating precursor in shock tubes. In: Grönig H (ed) Shock Tubes and Waves. VCH, Weinheim, New York, 847–853

Kuhl AL (1993) Turbulent Wall Jet in a Blast Wave Precursor In: Takayama K (ed) Japanese National Shock Wave Symposium. Tohoku University Press, Sendai, Japan

McGlaun JM, Thomson SL, Elrick MG (1990) CTH: a three-dimensional shock wave physics code. Int J Impact Engineering 10: 351–360

Mirels H (1988) Interaction of moving shock with thin stationary thermal layer. In: Grönig H (ed) Shock Tubes and Waves. VCH, Weinheim, New York, 171–183

Nemchinov IV, Bergelson VI, Orlova TI, Smirnov VA, Khazins VM (1987) Self-similar development of a precursor in front of a shock wave interacting with a thermal layer. Sov Phys Dokl 32: 691–692

Nemchinov IV, Artem'ev VI, Bergelson VI, Orlova TI, Rybakov VA, Smirnov VA, Khazins VM (1989) Formation of new structure in gas dynamic flows by disturbance of density in thin elongated channels ahead the shock waves. Mathematical Simulation vol.1 8: 1–11 (in Russian)

Nemtchinov IV, Artem'eva NA, Kosarev IB, Shuvalov VV, Svetsov VV, Neukum G, Hahn G, De Niem D (1997) Luminosity of the bolides created by SL-9 comet fragments in the Jovian atmosphere. Int J Impact Engineering 20: 591–599

Noh WF, Woodward P (1976) SLIC (simple line interface calculation). Springer Lecture Notes in Physics, 59: 330–340

Oran ES, Boris JP (1987) Numerical Simulation of Reactive Flow. Elsevier, New-York, 480–481

Rodionov AV (1996) Simulation of the outflow of three-dimensional multiphase jets from the surface of a cometary nucleus. Solar System Research, 30: 230–239

Rybakov VA, Nemchinov IV, Shuvalov VV, Artem'ev VI, Medveduk SA (1997) Mobilization of dust on the Mars surface by the impact of small cosmic bodies. JGR, 102: 9211–9220

Sadovsky MA, Adushkin VV (1988) Effect of a heated wall layer on shock wave characteristics. Docl Acad Nauk USSR 300: 3–12 (in Russian)

Samarsky AA, Popov YuP (1980) Finite Difference Methods for Gas Dynamic Problems. Nauka, Moscow, 101–108 (in Russian)

Shreffler RG, Christian RH (1954) Boundary disturbances in high-explosive shock tubes. J Appl Phys 25: 324

Shuvalov VV, Artem'eva NA, Kosarev IB, Nemtchinov IV, Trubetskaya IA (1997) Numerical simulation of the bolide phase of the impact of comet Shoemaker-Levy 9 fragments on Jupiter. Solar System Research, 31: 393–400

Tsikulin MA, Popov YeG (1977) Emitting properties of strong shock waves in gases. Nauka, Moskow, 85–94

Valentine GA, Wohletz KH (1989) Numerical Models of Plinian Eruption Columns and Pyroclastic Flows. Geophys Res, 10: 1867–1887

Van Leer B (1977) Towards the ultimate conservative difference scheme IV. A new approach to numerical convection. J Comput Phys, 23: 276–299